Self-Assembly Behavior of a Diblock Copolymer of Poly(1,1-dihydroperfluorooctyl acrylate) and Poly(vinyl acetate) in Supercritical Carbon Dioxide

Shuiqin Zhou and Benjamin Chu*

Department of Chemistry, State University of New York at Stony Brook, Long Island, New York 11794-3400

Received June 25, 1998

ABSTRACT: High-pressure laser light scattering experiments were performed to study the molecular association behavior of a diblock copolymer of poly(1,1-dihydroperfluorooctyl acrylate) and poly(vinyl acetate) in supercritical carbon dioxide. Both pressure-induced and temperature-induced micellization processes were observed over a pressure range of 90−552 bar and a temperature range of 25−75 °C, respectively. In sequence with increasing pressure at a fixed temperature, five regions appeared: (1) an insoluble solute appeared; (2) a small portion of the copolymer was dissolved to form unimers; (3) around the critical phase separation pressure region, some large aggregates were observed together with unimers; (4) over the critical phase separation pressure, very narrow size-distributed micelles in equilibrium with unimers were formed in the solution; (5) with a further increase in pressure, the micelles were gradually dissolved to form unimers; in the meantime, some anomalous large aggregates appeared around the critical micelle pressure. The appearance of the large aggregates can be ascribed to the copolymer composition heterogeneity. Upon lowering the temperature at a fixed pressure, a similar dissolution and association process of the copolymer in CO_2 was observed in terms of the critical phase separation temperature and the critical micelle temperature (CMT), because both increasing pressure and decreasing temperature increase the density of CO_2 and thus improve the solvent quality. The pressure dependence of the CMT with a fixed copolymer concentration, in combination with the pressure dependence of the critical micelle concentration at a fixed temperature, enables us to summarize the results with a mathematical relation among the critical micelle concentration, pressure, and temperature. After knowing either two of them for the copolymer solution in CO_2, the third critical micellization condition can be predicted. The positive standard enthalpy of micellization (+18.8 kJ/mol) indicates an entropy-driven process.

Introduction

Supercritical carbon dioxide has attracted a great deal of interest in recent years because it is viewed as a potentially important alternative to environmentally harmful chlorofluorocarbons (CFCs) and other organic solvents for use in chemical extraction, polymer synthesis, and industrial processing.[1−7] As a solvent, CO_2 is nontoxic, nonflammable, naturally abundant, easily disposable, and its critical point (T_c = 31 °C, P_c = 73.8 bar) is easily accessible. Moreover, the solvent quality can be tailored by changing the pressure or temperature. However, at present, industry is still using millions of tons of hazardous organic solvents a year because few substances will dissolve in CO_2. The recent development of surfactants designed specially to be amphiphilic in CO_2 may help CO_2 to dissolve many biomolecules and materials that are important to industry by means of emulsions, suspensions or dispersions.[8−12] Two types of block copolymer surfactants based on the poly(1,1-dihydroperfluorooctyl acrylate) (PFOA) block or the poly(dimethylsiloxane) (PDMS) block have been synthesized in the past few years.[12,13] It was anticipated that these amphiphilic block copolymers would self-assemble into micelles consisting of a CO_2-phobic core and a CO_2-philic corona when dissolved in supercritical or liquid CO_2, thereby creating useful microenvironments under controlled conditions for various specific purposes, such as synthetic and catalytic reactions, extractions of compounds, polymer processing and separation in supercritical or liquid CO_2.

The self-assembly of block copolymers can usually be initiated either by an increase in concentration via the critical micelle concentration (CMC) or by changing the temperature via the critical micelle temperature (CMT), above or below which the formation of associated structures becomes appreciably important.[14] In our laboratory, a series of studies have been carried out on the temperature-induced micellization of various block copolymers with different composition and chain architecture in common solvents.[15−20] The hydrophilic−hydrophobic characteristics of polymeric surfactant molecules could be considerably modified by changing the temperature. Similarly, the solvent quality for the block copolymers in supercritical fluids can be manipulated by simply changing the pressure or temperature. Many small-angle X-ray scattering (SAXS) and small angle neutron scattering (SANS) studies on the molecular dissolution/aggregation behavior of surfactants or polymers in supercritical fluids have been reported;[21−29] however, only a few laser light scattering (LLS) studies have been carried out for the microemulsions of conventional small surfactant molecules in supercritical fluids.[30−32] The high-pressure requirement of supercritical fluids made it very difficult experimentally to construct suitable light-transmitting windows. A sapphire window could depolarize the incident laser beam,[30−32] while an optical isotropic quartz glass window could be too brittle to be operated at high pressures (i.e., >350 bar).[33] The first high-pressure light scattering study on the pressure-induced micellization of a diblock copolymer has been performed in our labora-

10.1021/ma980990x CCC: $15.00
Published on Web 10/06/1998

tory,[34] by using a newly constructed high-pressure fiber-optic LLS spectrometer with gradient index of refraction microlenses as cell windows.[35] The use of the fiber-optic probes not only miniaturized the LLS spectrometer but also provided a high spatial coherence factor (β) value of 0.7−0.9.[35,36] The equipment has proven to be very useful in probing the self-assembly behavior of block copolymers in supercritical CO_2, especially for large aggregates over 100 nm, which have a length scale beyond the conventional SAXS or SANS experiments. The micelle formation and breaking-up, the micelle size and its distribution, the intensity contribution from each species, and some quantitative calculation from the CONTIN results can provide us with a clear picture about the pressure-induced molecular association process of the diblock copolymer in supercritical CO_2,[34] in terms of the critical micelle pressure (CMP).

On the basis of the previous LLS study on the pressure-induced self-assembly behavior of the diblock copolymer of poly(1,1-dihydroperfluorooctylacrylate) and poly(vinyl acetate) (PFOA-*b*-PVAC) in supercritical CO_2, we extend the pressure-induced micellization to a dilute solution. Meanwhile, the temperature-induced micellization of the copolymer in supercritical CO_2 at different pressures were also studied in this work. The knowledge about the CMC (or CMP or CMT) is of fundamental importance to predict the micellization ability under controlled experimental conditions. From the pressure dependence of CMC at a fixed temperature[34] and of CMT at a fixed concentration, a mathematical relation among the CMC, temperature, and pressure is proposed so that we can predict the CMC value at a known pressure and temperature for the PFOA-*b*-PVAC block copolymer in CO_2. Alternatively, we can predict a CMP at a known concentration and temperature, or CMT at a known concentration and pressure.

Experimental Section

Materials. SFC grade CO_2 for the LLS experiments was purchased from Scott Specially Gases. α,α,α-Trifluorotoluene (Aldrich, 99+%) was used as received. Vinyl acetate (VAC, Aldrich) and 1,1-dihydroperfluorooctyl acrylate (FOA, 3M) were purified and deinhibited by passage through an alumina column and were deoxygenated by argon purge prior to use. Benzyl *N*,*N*-diethyldithiocarbamate (BDC) was synthesized according to previously published literature.[13]

Synthesis of the PFOA-*b*-PVAC Diblock Copolymer. The block copolymer was synthesized using the iniferter polymerization technique by first polymerizing PVAC block using BDC as the iniferter in conjuction with UV light.[37] The diblock copolymer used in this paper was obtained from professor J. M. DeSimone at UNC at Chapel Hill. The sample had a molecular weight of 4.31×10^4 for the PFOA block and 1.03×10^4 for the PVAC block, respectively. The PVAC block had a polydispersity of $M_w/M_n = 1.6$.

High-Pressure Fiber-Optic LLS Instrumentation. The details of the instrumentation and its principles have been described elsewhere.[35] Briefly, the laboratory-built high-pressure LLS cell was machined from 316 stainless steel. Besides the incident and exit windows, three detectable windows were opened, giving access to 30°, 90°, and 150° scattering angles. Single or multiple fiber-optic probes, each comprising an optical fiber and a graded index microlens, were used to transmit the incident laser beam and to receive the scattered light from the high-pressure cell. Our fiber-optic probes positioned at different angles formed an integral part of the scattering cell. Thus, no transparent windows and goniometer were required. Such an arrangement has enabled us to use the microlens itself as the optical window in the high-pressure cell for LLS measurements. In the present setup, single fiber optic probes were used at 90° and 150°, while a multiple fiber optic probe with six fibers was used at 30°. The calibrated results for all of the eight fiber probes are located at 27.6°, 29.1°, 30.7°, 32.0°, 33.6°, 35.7°, 94.0°, and 146°, respectively. The total sample chamber volume could be varied from 2.4 to 6.0 mL. The inside surface of the cell was blackened to prevent light reflection. The sample in the cell could be stirred with a 12 × 7 mm, Teflon-coated magnetic stirring bar while the cell was put on the stirring plate. The pressure inside the cell was monitored by using an OMEGA-DYNE pressure transducer (TH-1) with a gauge meter (INFS-0001-DC1). The temperature of the cell was controlled by an OMEGA temperature controller (MODEL CN-76000) equipped with four OMEGA CSS cartridge heaters and a platinum RTD probe (PR-13).

High-Pressure LLS Measurements. A Spectra-Physics Model 165 argon ion laser operated at 488 nm was used as the light source. The PFOA-*b*-PVAC diblock copolymer used for high-pressure LLS measurements was dust-freed as follows: first, it was dissolved in α,α,α-trifluorotoluene at 2×10^{-3} g/mL, and then filtered carefully into a dust-free bottle by using 0.2 μm Millipore filters; finally, the solution was evaporated and vacuum-dried at 45 °C for 1 week. The high-pressure cell was dust-freed by flowing filtered supercritical CO_2 through the sample chamber for 1 h before use. A known amount of sample was added to the high-pressure cell from the exit window channel. After having heated the cell to the desired temperature, it was pressurized with CO_2 to the desired pressure. The light-scattering measurements were recorded after the solution had been stirred for 1−10 h and further equilibrated for 5−10 h, both depending on the working pressure and temperature. *Experiments were typically performed with a pressure and temperature precision of* ±0.5 bar and ±0.2 °C, respectively. Photon correlation measurements were carried out by using a Brookhaven Instruments digital correlator (BI9000). Normally, an intensity−intensity time correlation function $G^{(2)}(t,q)$ in the self-beating mode is measured. $G^{(2)}(t,q)$ has the following form[38,39]

$$G^{(2)}(t,q) = A[1 + \beta|g^{(1)}(t,q)|^2] \tag{1}$$

where A is a measured baseline, t is the delay time, and $g^{(1)}(t,q)$ is the normalized electric field time correlation function, which can be related to the line-width distribution $G(\Gamma)$ by

$$g^{(1)}(t,q) = \int_0^\infty G(\Gamma)e^{-\Gamma t}\, d\Gamma \tag{2}$$

A Laplace inversion of eq 2 gives $G(\Gamma)$, and the inversion can be accomplished by using a CONTIN program.[40] The line width (or relaxation rate) $\Gamma = Dq^2$, where D is the translational diffusion coefficient, and $q = (4\pi n/\lambda)\sin(\theta/2)$ with n, λ, and θ being the solvent refractive index, the wavelength of light in vacuo, and the scattering angle, respectively. After knowing the D value, we can further determine the (equivalent) hydrodynamic radius (R_h) by using the Stokes−Einstein relation

$$R_h = k_B T/6\pi\eta D \tag{3}$$

where k_B is the Boltzmann constant and η is the solvent viscosity. The experimental uncertainties for D and R_h are within ±3% for our instrument. It should be mentioned that both n and η[41] are pressure and temperature dependent for supercritical CO_2. In the present work, n is calculated by using the equation[42]

$$V\frac{n^2-1}{n^2+2} = 6.600 + \frac{1.25}{V} - \frac{264}{V^2} \tag{4}$$

where $V = M/\rho$ in mL/(g·mol) with M and ρ being the molar mass and density of CO_2, which can be found elsewhere.[43]

Results and Discussion

Pressure-Induced Micellization. Figure 1 shows the pressure dependence of the excess scattered inten-

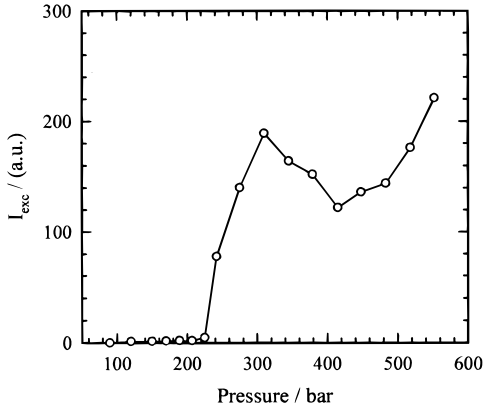

Figure 1. Plot of excess scattered intensity versus pressure for the diblock copolymer of PFOA-*b*-PVAC copolymer in supercritical CO_2 at $C = 24$ mg/mL, $T = 65$ °C, and scattering angle $\theta = 32°$.

sity for the PFOA-*b*-PVAC diblock copolymer in CO_2 at $C = 24$ mg/mL, $T = 65$ °C and a scattering angle θ of 32° over a pressure range of 90−552 bar. Here the excess scattered intensity (I_{exc}) is defined as the difference in the scattered intensity between the solution and the solvent, supercritical CO_2. I_{exc} is proportional to Δn, the difference of the refractive indices between the copolymer and the solvent ($\Delta n = n_P - n_S$ with n_P and n_S the refractive index of the copolymer and solvent, respectively). Six regions were observed in sequence with increasing pressure. (1) At very low pressures (<148 bar), nearly no scattered intensity was detected even though there is sufficient Δn value, indicating that the polymer did not dissolve in the supercritical CO_2 at such low pressures. (2) In the pressure range of 148−225 bar, the Δn decreased gradually with increasing pressure and showed very low values at 225 bar (∼+0.003). In terms of the relation of $I_{exc} \propto (\Delta n)^2$, I_{exc} should decrease. However, low excess scattered intensity was detected and I_{exc} increased with increasing pressure, indicating that a small portion of the copolymer was gradually dissolved to form unimers (single copolymer chains) in solution. (3) When the pressure was increased from 225 to 242 bar, the Δn value of the copolymer in supercritical CO_2 changed from +0.003 to −0.012. If the solution behavior were kept unchanged, an estimated increase of I_{exc} by a factor of about 16 should be observed due to the increase in Δn. The fact was that I_{exc} increased dramatically by a factor of about 20. This difference is significant because the experimental uncertainty for I_{exc} is within ±2%. As will be evidenced by the DLS results later, this intermediate region represents the dissolution and the micelle formation of the PFOA-*b*-PVAC copolymer in CO_2 around the critical phase separation pressure, defined as the pressure below which the polymer is essentially insoluble at the specified temperature. (4) With increasing pressure from 242 to 310 bar, the Δn value increased from +0.012 to +0.050 but was still very low. In principle, the I_{exc} should remain low but have an estimated increase by a factor of about 16. However, the detected I_{exc} was high in this region, and the intensity only increased by a factor of about 2 when the pressure was increased from 242 to 310 bar. As will be evidenced by DLS results, this is a region where the micelles were in equilibrium with the unimers, but the micelles became smaller with increasing pressure. (5) When the pressure was above 310 bar, the I_{exc} value decreased with increasing pressure until the pressure reached 415 bar although the Δn value increased continuously by about 70% with increasing pressure from 310 to 415 bar. Without the effect of Δn increase, the I_{exc} value should decrease more dramatically with increasing pressure. The decrease in the scattered intensity could be attributed to the gradual dissolution of micelles. With increasing pressure, CO_2 became a better solvent for both PFOA and PVAC blocks, and thus led to a weaker selectivity of solvation for the two blocks and a breakup of micelles. (6) At high pressures (415−552 bar), I_{exc} increased quickly with increasing pressure. Normally, the breakup of micelles should lead to a lower scattered intensity of solution. The unexpected higher scattered intensity in this region could be related to two reasons. One is the appearance of some anomalous large aggregates after the breakup of micelles. Another is the high Δn values between the copolymer and supercritical CO_2 at such high pressures (i.e., $\Delta n \sim 0.1$ at 518 bar). In comparison with the results obtained from higher concentration solutions,[34] it could be found that the first three regions did not show a concentration dependence over a concentration range of $C = 24$−97 mg/mL at 65 °C. This is reasonable because the critical phase separation condition must be the same for the same kind of polymer. However, the last two regions shifted toward lower pressures with decreasing solution concentration. The more dilute the solution, the lower the pressure at which the micelles started to be broken up and the large aggregates appeared. In other words, the critical micelle pressure (CMP) depends strongly on the solution concentration. The more dilute the solution, the lower the CMP value. It should be mentioned that the pressure dependence of I_{exc} discussed above was only limited in our experimental conditions of $C = 24$ mg/mL and $T = 65$ °C. The temperature change will definitely change the solvent quality and solvent refractive index of supercritical CO_2. Thus I_{exc} must show a different pressure dependence at different T and C. However, the general trend should be the same.[34]

Figure 2 shows plots of intensity contribution function versus (apparent) hydrodynamic radius for the PFOA-*b*-PVAC copolymer solution in CO_2 at $C = 24$ mg/mL, $\theta = 32°$, $T = 65$ °C and the indicated pressures. It should be mentioned that the angular dependence of the size distributions of the PFOA-*b*-PVAC copolymer solution at higher concentrations had been determined before.[34] The micelle species did not show apparent angular dependence. Thus, all of the DLS measurements for the hydrodynamic radius distributions are fixed at a scattering angle of 32° in this paper. The distribution function is expressed in arbitrary units but normalized to the highest value at each pressure to facilitate a comparison. In so doing, the peak area is a measure of the scattered intensity contribution but on a relative scale. At low pressures (148−170 bar), although the total scattered intensity was very low in Figure 1, DLS experiments still show us the presence of only narrowly distributed unimers with an average hydrodynamic radius $\langle R_h \rangle$ of ∼3 nm. In the pressure range of 189−225 bar, polydispersed large aggregates with $\langle R_h \rangle$ of hundreds of nanometers appeared in coexistence with the dissolved polymer chains. These large particles, being suspended in the solution, could be attributed to the undissolved copolymers, which might be stabilized by an adsorbed layer of dissolved unimers. Assuming that approximately $M \propto R^3$ and scattered intensity $I_{exc} \propto CM$, the large undissolved aggregates can be esti-

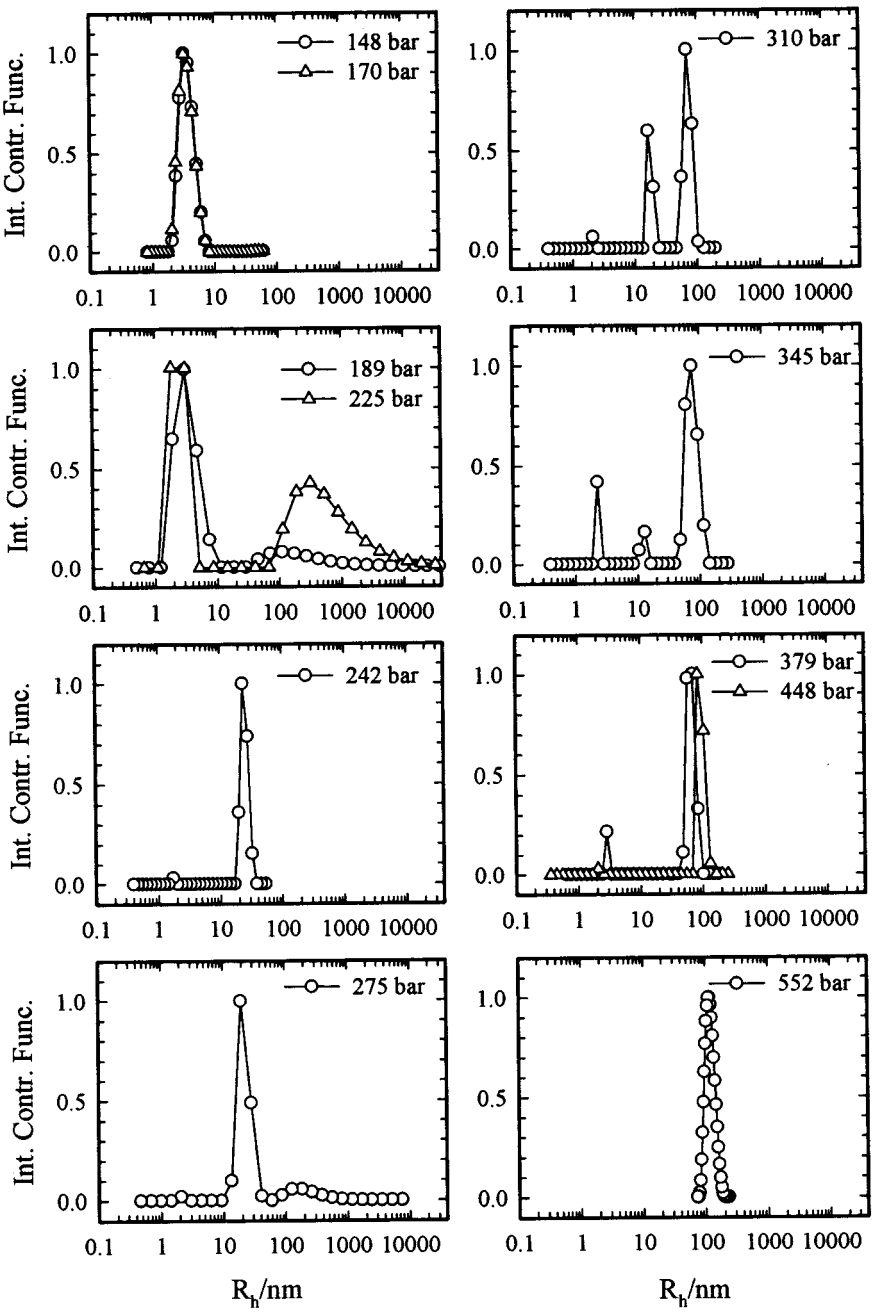

Figure 2. Intensity contribution function (i.e., $\Gamma G(\Gamma)$) versus (apparent) hydrodynamic radius R_h for the PFOA-*b*-PVAC copolymer in CO_2 at $C = 24$ mg/mL, $T = 65$ °C, $\theta = 32°$, and the indicated pressures. The peak area is proportional to the scattered intensity contribution.

mated to take only a few millionths in weight fraction at 225 bar (even less at 189−206 bar). Thus, the main species in the solution were the dissolved polymer chains. However, the total scattered intensity in Figure 1 over the pressure range of 189−206 bar was still very low, which indicated that only a portion of the copolymers was dissolved, and the solvent quality was still poor for the diblock copolymer under these pressures. When the pressure was increased from 206 to 225 bar, the total scattered intensity increased nearly three times, while Δn decreased by a factor of about 4, signifying an actual change in I_{exc} ($\propto CM$) by a factor of about 50. The scattered intensity from the unimers, as shown in Figure 2 for $P = 225$ bar was about half the total scattered intensity. Therefore, the dissolution of the copolymers became significant when the pressure reached 225 bar. It should be noted that the LLS results on the coexistence regime of unimers in the presence of undissolved large aggregates for the PFOA-*b*-PVAC copolymer in the pressure range of 189−225 bar at 65 °C (CO_2 density: 0.65−0.73 g/mL) are consistent with the results of an NMR study on the dissolution of PFOA homopolymer or PFOA-*b*-PS (polystyrene) diblock copolymer, where a coexistence regime of an unswollen polymer phase with a dissolved polymer phase was observed at 64.6 °C in the CO_2 density range of 0.55−0.72 for PFOA and 0.6−0.73 for PFOA-*b*-PS, respectively.[44] When the pressure was increased to 242 bar, very narrow size-distributed micelles were formed in equilibrium with unimers. Similar to the scattered intensity results, DLS results also showed that the PFOA-*b*-PVAC copolymer in CO_2 at low concentrations experienced the same dissolution/micelle-formation process as those at higher concentrations at pressures

below 242 bar.[34] However, when the pressure was over 275 bar, the dilute solution showed different DLS results in comparison with the more concentrated solutions; namely, the breakup of micelles and the appearance of the anomalous large aggregates shifted toward lower pressures. For the 24 mg/mL solution, a small amount of large aggregates first appeared at 275 bar. Then, the large particles took more and more contribution to the total scattered intensity with increasing pressure. In contrast, the micelles were gradually dissolved, resulting in smaller micelle size and smaller micelle peak area with increasing pressure. When the pressure reached 345 bar, the micelle peak became very small. Assuming that $M \propto R^3$ and $I_{exc} \propto CM$, the weight fraction of unimers, micelles, and large aggregates in the solution could be estimated to have a ratio of 2×10^2:1:0.06. Accordingly, the micelles and large aggregates only took a few thousandths fraction on the weight basis and the unimers were quantitatively overwhelming in the solution, even though the total scattered intensity was mainly contributed by the large aggregates. At 379 bar, the micelles disappeared completely. Approximately, the pressure value of 345 bar can be viewed as the CMP at $C = 24$ mg/mL and $T = 65$ °C. With a further increase in pressure, the size of the large particles increased. Although the unimers remained quantitatively overwhelming in the solution at high pressures, their relative contribution to the total scattered intensity was very small, i.e., less than one hundredth of the total scattered intensity. This explains why the unimer peak was also no longer visible in DLS experiments at high pressures (e.g., at 552 bar as shown in Figure 2).

The anomalous large aggregates before the onset of micellization have been reported for other types of block copolymers in common solvents.[14−16,18] Similarly, the large particles appearing around the CMP could be ascribed to the composition heterogeneity of the block copolymer. Some model calculations indicate that the composition inhomogeneity could be appreciable even for a copolymer with a narrow distribution of molecular weight.[45] There may exist a very small portion (e.g., a few thousandths on a weight basis) of the copolymer specimen having a higher content of the insoluble block. When the solvent quality becomes increasingly poorer by varying the pressure, the minor insoluble components will precipitate out before reaching the micellization conditions of the major component, thus resulting in the formation of a dilute dispersion of large colloidal particles stabilized by the adsorbed layer of the major component. When the micelle formation of the major component is initiated, the minor insoluble portion can either be incorporated into the micellar core or form mixed micelles. Consequently, after reaching the CMP, the large particles from the minor insoluble components contributed less and less to the total scattered intensity due to the formation of micelles with decreasing pressure. Finally, the large aggregates completely disappeared at 242 bar.

Figure 3 shows the time dependence of the hydrodynamic radius distributions of PFOA-*b*-PVAC copolymer solution in CO_2 at $C = 24$ mg/mL, $\theta = 32°$, and $T = 65$ °C after the pressure was increased from 310 to 345 bar (~CMP). The solution was stirred for 30 min and equilibrated for 1 h before recording the DLS data at $t = 2$ h. During the first 2 h, DLS experiments only showed two species corresponding to unimers and large aggregates, respectively. No micelle peak was detected. After standing at 345 bar for 15 h, a small micelle peak with an $\langle R_h \rangle$ of 11.7 nm appeared. Moreover, the size of the large particles became smaller with increasing equilibration time, probably due to the formation of micelles, which can incorporate some insolube components to the micellar core. Although the size of unimers remained exactly unchanged, the relative intensity contribution of unimers increased about 3 times after the long time equilibration. These results indicated that the micelle formation was relatively slow when pressure was near the CMP. The coexistence of two species (unimers and large particles) detected during the first 2 h was only in a kinetic state. Therefore, it is necessary to keep long enough equilibration time for the solution near the critical micellization condition in order to get reliable and reproducible results.

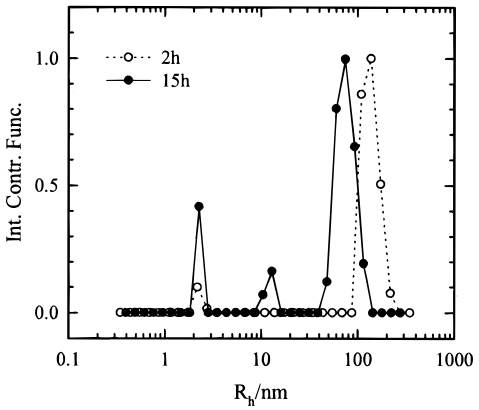

Figure 3. Time dependence of the hydrodynamic radius distributions for the PFOA-*b*-PVAC copolymer solution in CO_2 at $C = 24$ mg/mL, $T = 65$ °C, $\theta = 32°$, and $P = 345$ bar.

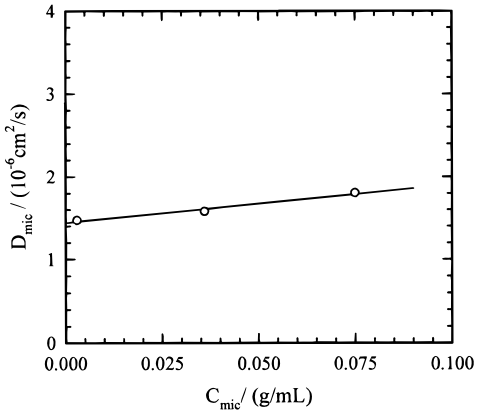

Figure 4. Plot of the mean diffusion coefficient of the micelle species versus the micellar concentration for the PFOA-*b*-PVAC copolymer solution in supercritical CO_2 at $C = 24$ mg/mL, $T = 65$ °C, $\theta = 32°$, and $P = 275$ bar.

Figure 4 shows the micellar concentration dependence of the micellar diffusion coefficient (D_{mic}) of the PFOA-*b*-PVAC copolymer solution in CO_2 at 65 °C and 275 bar. The D_{mic} values were taken from the mean values (*z*-average) of the corresponding micelle peaks. The CMC and D_{mic} data at two high concentrations were taken from previous work.[34] The D_{mic} at finite concentrations can be expressed as

$$D_{mic} = (D_{mic})_0 (1 + k_D C_{mic}) \quad (5)$$

where $(D_{mic})_0$ and k_D are the mean micellar diffusion coefficient at the CMC and the diffusion second virial

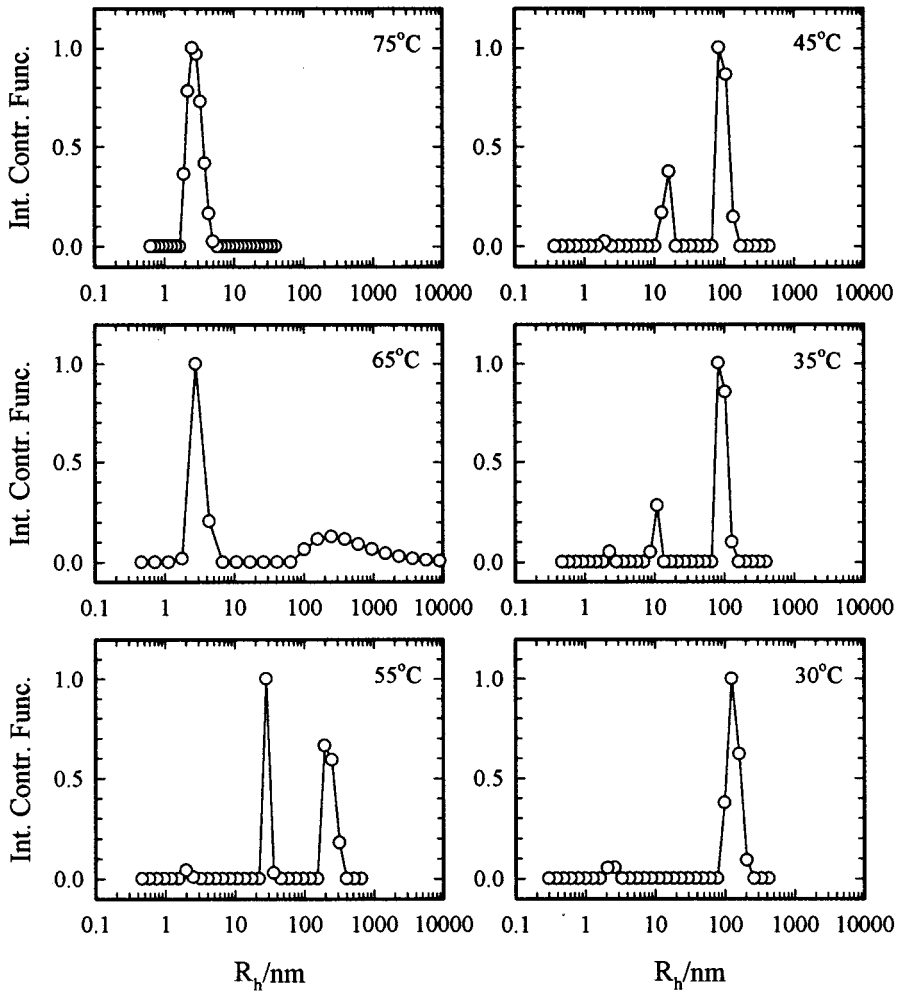

Figure 5. Intensity contribution function versus hydrodynamic radius R_h for the PFOA-*b*-PVAC copolymer in CO_2 at $C = 24$ mg/mL, $\theta = 32°$, $P = 225$ bar, and the indicated temperatures.

coefficient. The linear relation with a small positive slope gives $k_D = 3.2$ cm^3/g and $(D_{mic})_0 = 1.44 \times 10^{-6}$ cm^2/s. Correspondingly, the micelles have an average hydrodynamic radius $\langle R_h \rangle_0 = 22.0$ nm at CMC. By assuming that the micellar core consists of only the PVAC block and that all PVAC blocks reside in the micellar core, we can estimate the micellar core radius (R_c) value by using N and the relation

$$(4\pi/3)(R_c)^3 = (NM_{PVAC})/(N_A\rho_{PVAC}) \qquad (6)$$

where N is the aggregation number of micelles,[34] M_{PVAC} is the molecular weight of the PVAC block, N_A is Avogadro's constant, and ρ_{PVAC} is the density of PVAC, respectively. The estimated R_c value was equal to 4.0 nm. According to the spherical core−shell model for the micelles formed by a diblock copolymer, the difference between $\langle R_h \rangle_0$ and R_c is a measure of the corona thickness of the micelles. Thus, the micelles have a shell thickness $R_s = \langle R_h \rangle_0 - R_c = 18.0$ nm at 65 °C and 275 bar. On the basis of a C−C bond length of 1.54 Å and bond angle of 109.5° for a zigzag conformation chain,[46] the length of the FOA unit can be calculated as 2.5 Å. With a molecular weight of 4.31×10^4 for the PFOA block, the maximum stretched length of the PFOA block can be estimated to be ~23.8 nm. In comparison with this value, the measured corona thickness of 18.0 nm is reasonable.

Temperature-Induced Micellization. Figure 5 shows the size distributions in terms of R_h as a function of temperature for the PFOA-*b*-PVAC copolymer in CO_2 at $C = 24$ mg/mL, $\theta = 32°$, $P = 225$ bar, and the indicated temperatures. The DLS results showed a clear picture about the temperature-induced dissolution and association behavior for the copolymer in CO_2. In sequence with lowering temperature over a range of 75−30 °C, a narrowly distributed unimer peak was first observed at 75 °C; then, some polydispersed undissolved large aggregates together with the dissolved unimers were observed at 65 °C. By decreasing the temperature to 55 °C, three kinds of species with different sizes were present in the solution, corresponding to unimers, micelles, and large colloidal particles, respectively. With a further decrease in temperature, the micelles became smaller in size and contributed less to the total scattered intensity, while the large colloidal particles contributed more and more to the total scattered intensity. These results indicated that the micelles were gradually dissolved with decreasing temperature because the solvent quality became better for both blocks. When the temperature was lowered to 35 °C, the micelles could be estimated to constitute only 2% on a weight basis, as shown in Figure 5 (middle right panel). Further decreasing the temperature to 30 °C, the micelles were completely broken up to unimers. Although the unimer peak was quite small relative to the large particle peak, which made a major contribu-

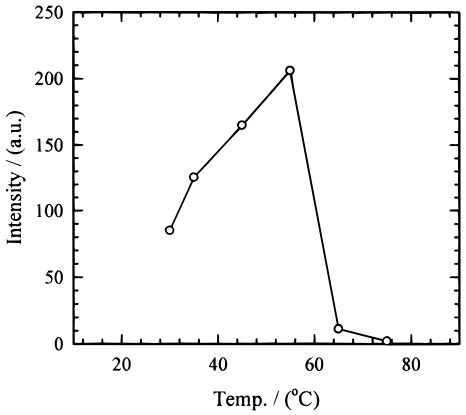

Figure 6. Plot of excess scattered intensity versus temperature for the PFOA-*b*-PVAC copolymer in CO_2 at $C = 24$ mg/mL, $\theta = 32°$, and $P = 225$ bar.

tion to the total scattering, the unimers were quantitatively overwhelming (in number) in the solution. After comparing the results at 35 and at 30 °C, the critical micelle temperature (CMT) for the PFOA-*b*-PVAC copolymer solution at $C = 24$ mg/mL and $P = 225$ bar can be estimated to be about 33 °C. When the temperature is above this value, the micelle formation becomes increasingly important and the large aggregates can be gradually incorporated into the micellar core. A comparison between Figure 5 and Figure 2 clearly showed that the dissolution/association processes of the PFOA-*b*-PVAC copolymer in CO_2 in sequence with decreasing temperature were in agreement with those in sequence with increasing pressure. Either decreasing temperature or increasing pressure improved the solvent quality of CO_2 for the PFOA-*b*-PVAC copolymer due to the increase of CO_2 density. Supposedly, a bimodal distribution region corresponding to the micelles in equilibrium with unimers could be observed in the temperature range of 65−55 °C. Unfortunately, the measurement was missed and we no longer have the same polymer sample to perform this experiment.

Figure 6 shows the temperature dependence of the excess scattered intensity for the PFOA-*b*-PVAC copolymer in CO_2 at $C = 24$ mg/mL, $\theta = 32°$, and $P = 225$ bar. Although the DLS measurements showed a narrowly distributed unimer peak at 75 °C, the total scattered intensity was very low, which indicated that only a very small portion of the polymer was dissolved at 75 °C. When the temperature was lowered to 65 °C, the total scattered intensity increased by about 6 times. Even though a small amount of large undissolved aggregates suspended in the solution contributed to the scattering, most of the intensity increase was from the unimers, which indicated that the copolymers were almost dissolved at 65 °C. By lowering the temperature to 55 °C, the scattered intensity increased dramatically because of the formation of micelles and large particles. When the temperature further decreased from 55 to 30 °C, the intensity decreased. The decrease in the scattered intensity was mainly due to the gradual dissolution of micelles as the solvent quality became better for the copolymer with decreasing temperature.

Figure 7 shows a similar temperature-induced micellization process in terms of hydrodynamic radius distributions for the PFOA-*b*-PVAC solution in CO_2 at $C = 24$ mg/mL, $\theta = 32°$, and $P = 242$ bar. The dissolution process of the copolymer in CO_2 was not followed any more at high temperatures. However, a normal micellization region, which was missed at 225 bar in Figure 5, was clearly observed at 242 bar and 65 °C, as a narrow bimodal distribution corresponding to micelles and unimers, respectively. It is noted that the unimers were hardly observable, as expected. When the temperature was lowered to 55 °C, a small amount of anomalous large aggregates appeared, but the micelles still provided the main contribution to the total scattering. With a further decrease in temperature, the large aggregates contributed more and more to the total scattered intensity, while the micelles became smaller in size and contributed less to the total scattering. At 40 °C, the micelles were estimated to take only about 4% on the weight basis. At 35 °C, the micelles were completely dissolved. The unimers were also no longer detectable by DLS experiments due to their relatively small intensity contribution to the total scattering even though the unimers could be quantitatively overwhelming in the solution. Approximately, 37 °C can be viewed as the CMT value at 242 bar. In comparison with the results from Figure 5, it can be found that the CMT increased with increasing pressure for a solution at a fixed concentration.

Figure 8 shows the temperature dependence of the hydrodynamic radius distributions around the CMT for the 24 mg/mL PFOA-*b*-PVAC copolymer solution in CO_2 at $\theta = 32°$ and pressures of 415 and 483 bar, respectively. Similar to the temperature-induced micellization behavior in Figures 5 and 7, three kinds of species, corresponding to unimers, micelles, and anomalous large aggregates, respectively, were observed around the CMT. The micelles were gradually dissolved with decreasing temperature. At 415 bar, the micelles became very small in size with an $\langle R_h \rangle$ of 6.7 nm and only contributed about 5% to the total scattered intensity at 70 °C, which indicates that the association number of micelles has become very small under this condition. When lowering the temperature to 65 °C, the micelles were completely broken up. Thus, the CMT can be estimated to have a value of about 68 °C at 415 bar. When the pressure was increased to 483 bar, the micelles were broken up at even higher temperatures. At 75 °C, the micelles showed a relatively broad size distribution and an $\langle R_h \rangle$ of about 5 nm, which were only a little bit larger than the size of unimers. The small micelles disappeared completely at 70 °C. We can take 75 °C as the approximate CMT value for the solution at 483 bar.

Relation among the Critical Micelle Temperature, Pressure, and Concentration. First, as experimentally evidenced above, for a solution with a fixed concentration, the CMT values strongly depend on the pressure. The higher the pressure, the higher the CMT value. Figure 9 summarizes a plot of pressure against the reciprocal of (absolute) critical micelle temperature for the 24 mg/mL PFOA-*b*-PVAC solution in CO_2. A good linear relationship was obtained. The least-squares fit yields an expression

$$P = 2.28 \times 10^3 - 6.30 \times 10^5[1/(\mathrm{CMT})] \qquad (7)$$

with P and T expressed in units of bars and K, respectively. Second, our previous results[34] on the pressure dependence of CMC values for the same copolymer in CO_2 at 65 °C has shown a relation

$$\ln(\mathrm{CMC}) = 3.58 \times 10^{-3}P - 8.82 \qquad (8)$$

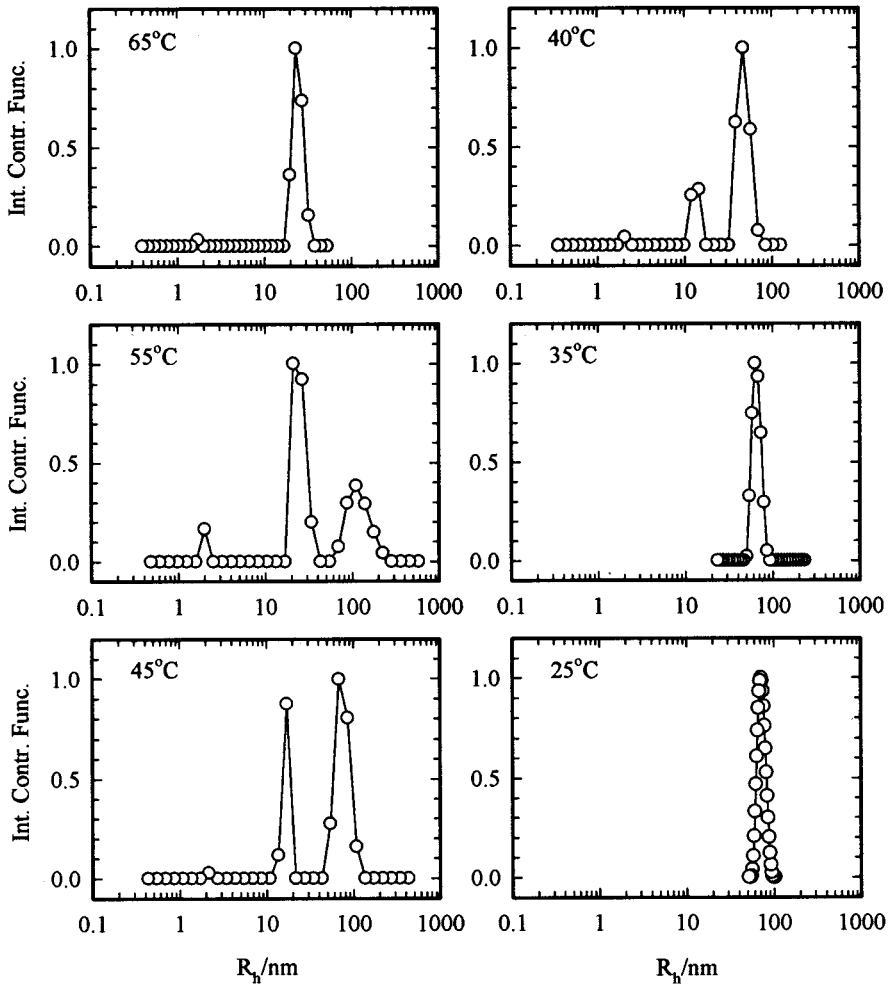

Figure 7. Hydrodynamic radius distributions for the PFOA-*b*-PVAC copolymer solution in CO_2 at $C = 24$ mg/mL, $\theta = 32°$, $P = 242$ bar, and the indicated temperatures.

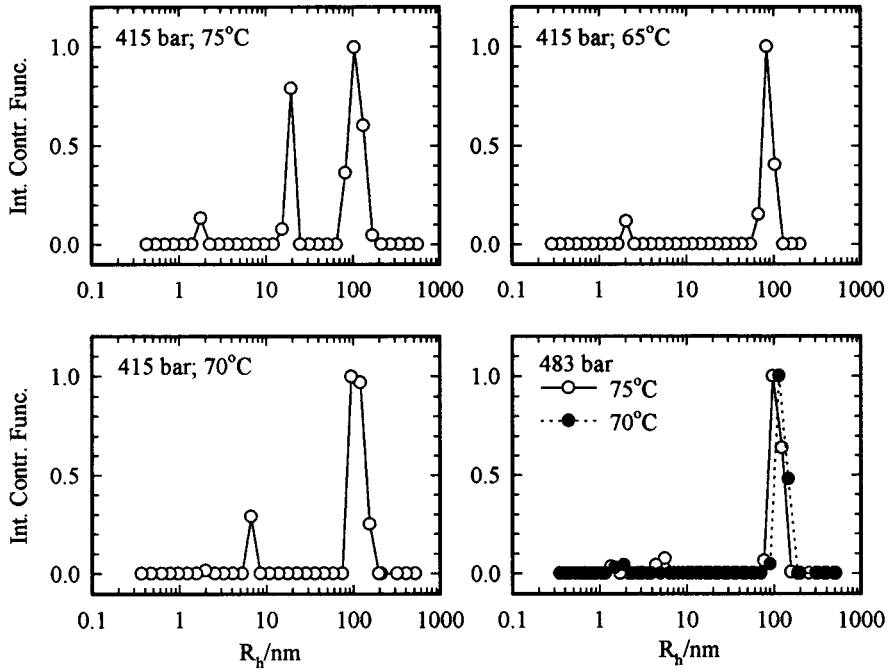

Figure 8. Temperature dependence of hydrodynamic radius distribution for the PFOA-*b*-PVAC copolymer solution in CO_2 at $C = 24$ mg/mL, $\theta = 32°$, and two different pressures of 415 and 483 bar, respectively.

where the CMC is in molar concentration. Third, for a closed association mechanism with relatively large association number and a narrow (size) distribution at a fixed pressure, the standard free energy and standard

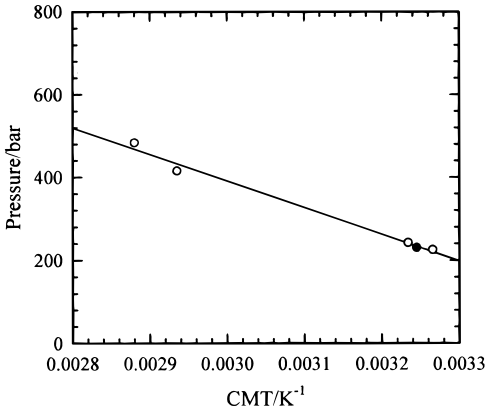

Figure 9. Plot of pressure versus reciprocal of the critical micelle temperature for the PFOA-*b*-PVAC solution in CO_2 at a fixed concentration C of 24 mg/mL. The filled circle denotes the CMP value at 35 °C.

enthalpy of micelle formation ($\Delta G°$ and $\Delta H°$, per mole of the solute in the micelle) can be calculated from the temperature dependence of CMC values by assuming that $\Delta H°$ is temperature independent.[47]

$$\Delta G° = RT \ln(\text{CMC}) \tag{9}$$

$$\Delta H° = R[\text{d} \ln(\text{CMC})/\text{d}(1/T)] \tag{10}$$

The two standard states are the polymer molecules and micelles in an ideal dilute solution at unity molarity. Equation 9 can be integrated to yield

$$\ln(\text{CMC}) \cong \Delta H°/(RT) + \text{const} \tag{11}$$

After considering the relation of variables in eqs 7, 8, and 11, a mathematical relation among the CMC, P, and T could be summarized in the following form

$$\ln(\text{CMC}) \cong a/T + bP + d \tag{12}$$

provided that a, b, and d are approximately constant in the temperature and pressure interval of interest. Thus, at a fixed concentration, a plot of CMP versus $1/T$ or P versus 1/(CMT) shows a linear relation; at a fixed temperature, ln(CMC) versus P shows a linear relation, and at a fixed pressure, ln(CMC) versus $1/T$ shows a linear plot. By replacing eq 7 at $C = 24$ mg/mL and eq 8 at $T = 65$ °C to eq 12, we can get $a = 2.26 \times 10^3$ and $b = 3.58 \times 10^{-3}$. However, the d value from eq 7 is slightly different from that with eq 8, namely, $d = -15.8$ by eq 7 and $d = -15.5$ by eq 8 were obtained, respectively. Considering the uncertainties of CMC values[34] (calculated from DLS results) used in eq 8 and of CMT values (determined from experiments) used in eq 7, the slight discrepancy is within the experimental uncertainties and is therefore acceptable. After knowing a, b, and d values, we can write eq 12 as

$$\ln(\text{CMC}) \cong 2.26 \times 10^3(1/T) + 3.58 \times 10^{-3}P - 15.8 \tag{13}$$

with CMC and P expressed in units of mol/L, and bar, respectively. Therefore, for the PFOA-*b*-PVAC copolymer (43.1k/10.0k) in CO_2, we can predict the critical micellization condition by knowing two of the three parameters. Although some assumptions have been used to simplify the calculation, eq 13 can provide us with a quantitative (or at least semiquantitative) understanding about the micellization behavior for a diblock copolymer in supercritical CO_2, where both pressure and temperature change can affect the solvent quality. Although eq 13 was derived specifically for the system of PFOA-*b*-PVAC diblock copolymer in supercritical CO_2, the format should be applicable in predicting the self-assembly behavior of all diblock copolymers in supercritical fluid, except for the numerical values of the coefficients (a, b, d), which should be system dependent. It should be mentioned that the physical meaning of constant a is related to $\Delta H°$. From $\Delta H°/R = a = 2.26 \times 10^3$ K, the standard enthalpy of micellization was found to be +18.8 (±2) kJ/mol, indicating that the micelle formation is an endothermic process. Within the solution region, the higher the temperature, the greater the micellization ability of the diblock copolymer in CO_2. The CO_2-phobic interactions of entropy origin from the PVAC blocks in CO_2 are mainly responsible for the micelle formation, meaning that the micellization process is entropy-driven.

Conclusions

Both pressure and temperature change can induce the micellization of PFOA-*b*-PVAC diblock copolymer in supercritical CO_2. A similar dissolution and association process of the copolymer in CO_2 was observed in sequence with increasing pressure and in sequence with decreasing temperature because of the increase of CO_2 density. During the process, five regions appeared: (1) solute; (2) very small portion of copolymer dissolved; (3) around the critical phase separation region, some undissolved large aggregates together with unimers; (4) normal micelle region presented as narrowly distributed micelles in equilibrium with unimers; (5) micelles gradually dissolved to unimers, and some anomalous large aggregates appearing around the critical micelle pressure or temperature. The large particles were caused by the copolymer heterogeneity. The dependence of the critical micelle concentration on pressure and temperature can be summarized by the relation $\ln(\text{CMC}/(\text{mol L}^{-1})) \cong 2.26 \times 10^3 ((1/T)/\text{K}^{-1}) + 3.58 \times 10^{-3}P/\text{bar} - 15.8$. After knowing two parameters, we can predict the third parameter. The positive standard enthalpy indicated an entropy-driven micellization process for the PFOA-*b*-PVAC copolymer in supercritical CO_2.

Acknowledgment. B.C. gratefully acknowledges the support of this work by the U.S. Department of Energy (DEFG 0286ER45237.013). He also wishes to thank the National Science Foundation (INT-9515361) for starting the project and the DuPont Co. for an unrestricted grant for laser repair and Professor J. M. DeSimone, at the University of North Carolina at Chapel Hill, for a sample of the PFOA-*b*-PVAC diblock copolymer.

References and Notes

(1) Kaiser, J. *Science* **1996**, *274*, 2013.
(2) Black, H. *Environ. Sci. Technol.* **1996**, *30*, 125A.
(3) Kiran, E., Levelt Sengers, J. M. H., Eds. *Supercritical Fluids: Fundamentals for Applications*; Kluwer: Dordrecht, The Netherlands, 1994.
(4) Lehotay, S. J.; Eller, K. I. *J. AOAC Int.* **1995**, *78*, 821.
(5) Lehotay, S. J.; Ibrahim, M. A. *J. AOAC Int.* **1995**, *78*, 445.
(6) Desimone, J. M.; Guan, Z.; Elsbernd, C. S. *Science* **1992**, *257*, 945.
(7) Canelas, D. A.; DeSimone, J. M. *Adv. Polym. Sci.* **1997**, *133*, 104 and references therein.

(8) Shaffer, K. A. Jones, T. A.; Canelas, D. A.; DeSimone, J. M. *Macromolecules* **1996**, *29*, 2704.
(9) Johnston, K. P.; Harrison, K. L.; Clarke, M. J. Howdle, S. M.; Heitz, M. P.; Bright, F. V.; Clarlier, C.; Randolph, T. W. *Science* **1996**, *271*, 624.
(10) Beckman, E. J. *Science* **1996**, *271*, 613.
(11) O'Neil, M. L.; Yates, M. Z.; Harrison, K. L.; Johnson, K. P.; Canelas, D. A.; Betts, D. E.; DeSimone, J. M.; Wilkinson, S. P. *Macromolecules* **1997**, *30*, 5050.
(12) Canelas, D. A.; DeSimone, J. M. *Macromolecules* **1997**, *30*, 5673.
(13) Guan, Z.; DeSimone, J. M. *Macromolecules* **1994**, *27*, 5527.
(14) Chu, B.; Zhou, Z. In *Nonionic Surfactants: Polyoxyalkylene Block Copolymer*; Nace, V. M., Ed.; Marcel Dekker: New York, 1996; Chapter 3.
(15) Zhou, Z.; Chu, B. *J. Colloid Interface Sci.* **1988**, *126*, 171.
(16) Zhou, Z.; Chu, B. *Macromolecules* **1988**, *21*, 2548.
(17) Zhou, Z.; Chu, B.; Peiffer, D. G. *Macromolecules* **1993**, *26*, 1876.
(18) Zhou, Z.; Chu, B.; Peiffer, D. G. *Langmuir* **1995**, *11*, 1956.
(19) Zhou, Z.; Chu, B.; Nace, V. M. *Langmuir* **1996**, *12*, 5016.
(20) Liu, T.; Zhou, Z.; Wu, C.; Chu, B.; Schneider, D. K.; Nace, V. M. *J. Phys. Chem. B* **1997**, *101*, 8808.
(21) McClain, J. B.; Londono, D.; Combes, J. R.; Romack, T. J.; Canelas, D. A.; Betts, D. E.; Wignall, G. D.; Samulski, E. T.; DeSimone, J. M. *J. Am. Chem. Sci.* **1996**, *118*, 917.
(22) Ritter, J. M.; Palavvra, A. M. F.; Kao, C. P. C.; Paulaitis, M. E. *Fluid Phase Equilib.* **1990**, *55*, 173.
(23) Kaler, E. W.; Billman, J. F.; Fulton, J. L.; Smith R. D. *J. Phys. Chem.* **1991**, *95*, 458.
(24) Zielinski, R. G.; Paulaitis, M. E.; Kaler, E. W. *Rev. Sci. Instrum.* **1996**, *67*, 2612.
(25) Fulton, J. L.; Pfund, D. M. In *Proceedings of Third International Symposium on Supercritical Fluids*; Perrut, Ed.; Strusburg, France, 1994; p. 391.
(26) Fulton, J. L.; Pfund, D. M.; Smith, R. D.; Carnaham, N. F.; Quintero, L.; Capel, M.; Leontaritis, K. *Langmuir* **1993**, *9*, 2035.
(27) Fulton, J. L.; Pfund, D. M.; McClain, J. B.; Romack, T. J.; Maury, E. E.; Combes, J. R.; Samulski, E.; deSimone, J. M.; Capel, M. *Langmuir* **1995**, *11*, 4241.
(28) Chillura-Martino, D.; Triolo, R.; McClain, J. B.; Combes, J. R.; Betts, D. E.; Canelas, D. A.; DeSimone, J. M.; Samulski, E. T.; Cochran, H. D.; Londono, J. D.; Wignall, G. D. *J. Mol. Struct.* **1996**, *383*, 3.
(29) McClain, J. B.; Betts, D. E.; Canels, D. A.; Samulski, E. T.; DeSimone, J. M.; Londono, J. D.; Cochran, H. D.; Wignall, G. D.; Chillura-Martino, D.; Triolo, R. *Science* **1996**, *274*, 2049.
(30) Fulton, J. L.; Blitz, J. P.; Tingey, J. M.; Smith, R. D.*J. Phys. Chem.* **1989**, *93*, 4189.
(31) Smith, R. D.; Fulton, J. L.; Blitz, J. P.; Tingey, J. M. *J. Phys. Chem.* **1990**, *94*, 781.
(32) Beckman, E. J.; Smith, R. D. *J. Phys. Chem.* **1990**, *94*, 3729.
(33) Kojima, J.; Takenaka, M.; Nakayama, Y.; Hashimoto, T. *Rev. Sci. Instrum.* **1995**, *66*, 4066.
(34) Zhou, S. Q.; Chu, B. *Macromolecules* **1998**, *31*, 5300.
(35) Zhou, S. Q.; Chu, B.; Dhadwal, H. S. *Rev. Sci. Instrum.* **1998**, *69*, 1955.
(36) Dhadwal, H. S.; Chu, B. *Rev. Sci. Instrum.* **1984**, *60*, 845.
(37) Betts, D.; Johnson, T.; Anderson, C.; DeSimone, J. M. *Polymer. Prepr. (Am. Chem. Soc., Div. Polym. Chem.* **1997**, *38*, 760.
(38) Pecora, R. *Dynamic Light Scattering*; Plenum Press: New York, 1976.
(39) Chu, B. *Laser Light Scattering*, 2nd ed.; Academic Press: New York, 1991.
(40) Provencher, S. W. *Makromol. Chem.* **1979**, *180*, 201; *Comput. Phys. Commun.* **1982**, *27*, 213.
(41) Stephan, K.; Lucas, K. *Viscosity of Dense Fluids*; Plenum Press: New York, 1979.
(42) Besserer, G. J.; Robinson, D. B. *J. Chem. Eng. Data* **1973**, *18*, 137.
(43) Angus, S.; Armstrong, B.; DeReuck, K. M. *International Thermodynamic Tables of the Fluid State: Carbon Dioxide*; IUPAC, Pergamon Press: New York, 1976.
(44) Dardin, A.; Cain, J. B.; DeSimone, J. M.; Johnson, C. S., Jr.; Samulski, E. T. *Macromolecules* **1997**, *30*, 3593.
(45) Kotaka, T.; Donkai, N.; Ik, T. *Min. Bull. Inst. Chem. Res. Kyoto Univ.* **1974**, *52*, 232.
(46) Tadokoro, H. *Macromol. Rev.* **1967**, *1*, 119.
(47) Lindaman, B.; Wennerstrom, H. *Top. Curr. Chem.* **1980**, *87*, 1.

MA980990X